

# Combined Use of Sentinel-1 and Sentinel-2 for Glacier Mapping: An Application Over Central East Alps

Riccardo Barella , Mattia Callegari , Carlo Marin , Christoph Klug , Rudolf Sailer, Stephan P. Galos, Roberto Dinale, Marco Gianinetto, and Claudia Notarnicola , *Senior Member, IEEE*

**Abstract**—The systematic monitoring of glaciers is essential to both evaluate water resource availability and better understand the effects of climate change. The increased speed of glacier changes observed in the past few years requires a more frequent update of the glacier inventories than in the past; however, the high human supervision required by the state-of-the-art techniques is discouraging their systematic application over large areas. This article proposes a novel approach to exploit the large volume of data provided by Copernicus Sentinel missions for detecting glacier outlines, including debris-covered glaciers. In detail, our method exploits the Sentinel-1 and Sentinel-2 multitemporal images to build a composite image representing the glacier conditions during the yearly maximum ablation period. The Sentinel-2 multispectral images are classified with a support vector machine and composed to a mosaic that represents the information of the maximum glacier ablation. At the same time, the Sentinel-1 time series are exploited to build a multitemporal coherence composite that represents all the snow-covered and glaciated areas together with all the moving surfaces. This information is used together with the Sentinel-2 composite to detect the debris-covered part of the glaciers. The proposed method was tested in the Central East Alps and presented an overall accuracy of 92% with respect to a reference inventory over South Tyrol and an agreement of 90% with respect to the latest glacier inventory of the Alps from Sentinel-2. The proposed approach enables to assist glacier experts in identifying glacier outlines over large areas and in short time.

**Index Terms**—Copernicus, data assimilation, debris-covered glaciers, glacier monitoring, machine learning, Sentinel-1, Sentinel-2.

## I. INTRODUCTION

THE glaciers are an essential part of the hydrological cycle in the Alps, and their retreat is one of the most evident effects of climate change [1]. Glacier ice melting changes the water economy of many glacierized areas: reduced water availability for human consumption, agriculture, and hydropower production are negatively impacting glacier-driven catchments [2]. Glacier inventories are one of the most important information for glacier monitoring, and therefore, they are largely exploited. Glacier outlines are used for the estimation of key glaciological parameters, such as the glacier length, useful for understanding glacier trends [3], [4], and the accumulation area ratio [5], from which glacier mass balance can be derived [6]. Moreover, glacier outlines are also required for ice thickness modeling [7], [8], glacier mass balance estimation, and hydrological modeling [9]. Given the alpine glaciers' average size, Terra/ASTER and Landsat/TM/ETM+/OLI data were widely used in the last 30 years to monitor their extent [10], [11]. Specifically, Terra has collected 30-m spatial resolution images in 14 spectral bands since 2000 via the ASTER sensors, and the Landsat program has a massive archive of 30-m spatial resolution images, using TM, ETM+, OLI, and TIR sensor. Both the missions have a revisit time of 16 days and are a rich source of information to monitor the glacier changes on a global scale in the last 35 years. Generally, state-of-the-art methods that exploit optical imagery rely on human supervision [11]–[16]. For example, a glacier expert who delineates the glacier outlines on a wide area must browse the catalogue of historical images to search for cloud-free acquisitions with minimum snow coverage on each glacier (i.e., the condition of the maximum ablation of the glacier). The archived images that satisfy both the requirements are considered the optimal acquisitions for extracting the glacier outline by thresholding one or more spectral indices [11], [15]. Selecting the optimal images may be impossible for some years or particular glaciers due to cloud coverage. Moreover, the mapping of the debris-covered part of the glaciers is a complex task. Indeed, glaciers can be partially or even completely covered by rocky debris, which cannot be appropriately mapped using only multispectral images since the spectral signatures of rocks covering the glacier are mostly identical to those of the surrounding rock [16]. To overcome this problem, glacier experts are relying on very high-resolution images, which are,

Manuscript received October 5, 2021; revised March 29, 2022 and May 3, 2022; accepted May 11, 2022. Date of publication May 30, 2022; date of current version June 24, 2022. This work was supported in part by the Interreg ITAT 2025 GLISTT Project, for the development of an inter-regional system for glacier monitoring for the Tyrol and South Tyrol region. (*Corresponding author: Riccardo Barella.*)

Riccardo Barella, Mattia Callegari, Carlo Marin, and Claudia Notarnicola are with the Institute for Earth Observation, Eurac Research, 39100 Bolzano, Italy (e-mail: riccardo.barella@eurac.edu; mattia.callegari@eurac.edu; carlo.marin@eurac.edu; claudia.notarnicola@eurac.edu).

Christoph Klug, Rudolf Sailer, and Stephan P. Galos are with the Institute of Geography, University of Innsbruck, 6020 Innsbruck, Austria (e-mail: christoph.klug@uibk.ac.at; rudolf.sailer@uibk.ac.at; stephan.galos@gmail.com).

Roberto Dinale is with the Autonomous Province of Bolzano—South Tyrol, 39100 Bolzano, Italy (e-mail: roberto.dinale@provincia.bz.it).

Marco Gianinetto is with the Politecnico di Milano, 20133 Milano, Italy (e-mail: marco.gianinetto@polimi.it).

Digital Object Identifier 10.1109/JSTARS.2022.3179050

in general, specifically acquired for this purpose. Very high resolution images are classified on the basis of experts' knowledge, requiring a high amount of time. As a consequence, some authors proposed to map the glacier surface with synthetic aperture radar (SAR) images [17]–[20]. Using the interferometric coherence derived by SAR time series, it is possible to detect the debris-covered part of the glaciers [19]. The interferometric coherence provides information on both the land cover and ground displacements. However, to properly identify debris-covered glaciers, the coherence loss due to their displacement must be isolated from the coherence loss due to land cover type. Moreover, SAR images are insensitive to the cloud presence, so it is easier to catch the seasonal glaciers' maximum ablation. The Copernicus Sentinel program, which started with the acquisition of the first SAR image in 2014, has significantly increased the monitoring capabilities of the glaciers extent in the alpine region. Sentinel-1 and Sentinel-2 now guarantee systematic acquisitions with a nominal revisit time of six days for the SAR images and five days for multispectral images. Thus, the state-of-the-art methods are not suitable to process large data volume generated by Copernicus. Furthermore, this limitation is becoming more and more critical since inventories need to be updated more often than every ten years [21] due to the acceleration of glacier melting. This article proposes a novel approach for the automatic mapping of glaciers, including bare ice, accumulation area, and debris-covered glaciers. The method provides glacier outlines for large alpine areas, exploiting multitemporal composite of both Sentinel-1 and Sentinel-2 time series. The whole procedure is based on a limited human intervention. Several multitemporal composite techniques have been developed in the past especially in the field of vegetation monitoring using optical data to compose a cloud-free mosaic [22]–[25]. The main idea is to compose pixels of images acquired at different times to create a synthetic image representing the optimal situation for identifying a particular phenomenon and to filter out unwanted noise (e.g., clouds). To the best of our knowledge, the multitemporal composite technique was never applied in the context of glacier mapping. In this article, we propose to use Sentinel-2 time series to compose a cloud-free multispectral mosaic, made up of pixels of the images that better represent the maximum ablation of a particular glacier. On the other side, the Sentinel-1 SAR time series is used to derive information about the debris-covered part of the glacier. In the literature, we can find examples of land cover mapping methods that rely on features extracted by coherence's time series [26]–[28]. These methods are based on the fact that different land covers have different temporal patterns of the coherence. In our case, we do not use features extracted by the multitemporal information, but we keep only the meaningful information for debris-covered glacier mapping. In detail, a coherence composite is produced by taking the maximum of all the interferometric coherence calculated from each image pair with a defined temporal baseline. In fact, by taking the maximum coherence of the time series pixelwise, we are able to isolate the coherence losses due to permanent movements. Precisely, the glacier flow, even if covered by debris, can be separated from possible transient causes, such as the seasonal snow cover or rock falls. For reducing layover and shadow

effects, we use the information acquired from different orbits. The different orbits are processed separately, aligned to the same extent, and in the end, the maximum coherence value for each orbit goes in the final composite. Finally, the Sentinel-1 SAR coherence composite is used in combination with the optical multitemporal composite to map surface deformations caused by debris-covered ice flow. The main novelties of our approach are as follows: 1) the generation of a cloud-free multitemporal composite of Sentinel-2 images representing the maximum ablation status for each glacier; 2) the generation of a multitemporal and multiorbit composite that describes the maximum coherence used to identify the debris-covered part of glaciers; and 3) the synergistic exploitation of SAR and multispectral composites for glacier outline retrieval at maximum ablation. The method is tested in the Central East Alps (i.e., Sentinel-2 tiles 32TQS, 32TPS, 32TNS, 32TQT, 32TPT, and 32TNT) for 2015, 2016, and 2017. In detail, over South Tyrol, the results have been validated with the reference glacier inventory produced with state-of-the-art methods using aerial orthophotos and airborne laser scanner (ALS) digital elevation models relative to the years 2016 and 2017 by expert glaciologists. For the whole Central East Alps, a detailed intercomparison has been done with the glacier inventory of the Alps, extracted using Sentinel-2, and available for the year 2015 [16], which represents the most reliable and updated inventory over the Alps up to date.

## II. STUDY AREA AND DATASET

### A. Study Area

The method has been applied in the central and eastern Alps in the area defined by the footprint of six Sentinel-2 tiles, named using the UTM convention (32TQS, 32TPS, 32TNS, 32TQT, 32TPT, and 32TNT). This region includes a glaciated area of 608.2 km<sup>2</sup> according to the latest available glacier inventory relative to the year 2015 [see Fig. 1(a)]. In detail, inside this macroregion, we focused on the South Tyrol region, for which we have a high-resolution glacier inventory, edited by expert glaciologists [see Fig. 1(b)].

South Tyrol is an Italian mountain region at the border with Austria. It has an extension of 7397 km<sup>2</sup>, of which glaciers cover 84 km<sup>2</sup>, according to the high-resolution reference glacier inventories of 2016 and 2017. For our analysis, we split the territory into the following three independent study areas: 1) the Ortler Alps; 2) the Ötztal Alps; and 3) Zillertaler Alps and the Rieserferner Group. These three areas were selected to validate the method over different mountain groups and have metrics from three independent areas.

### B. Dataset

Sentinel-2 images are provided in tiles, each covering a square area of 10 000 km<sup>2</sup>. Thus, South Tyrol is covered by three tiles, while the whole study area is covered by six tiles, i.e., about 360 000 km<sup>2</sup>. Regarding South Tyrol, the Ortler Alps are included in tile 32TPS, the Ötztal Alps are included in tiles 32TPS and 32TPT, and the Zillertaler Alps and the Rieserferner

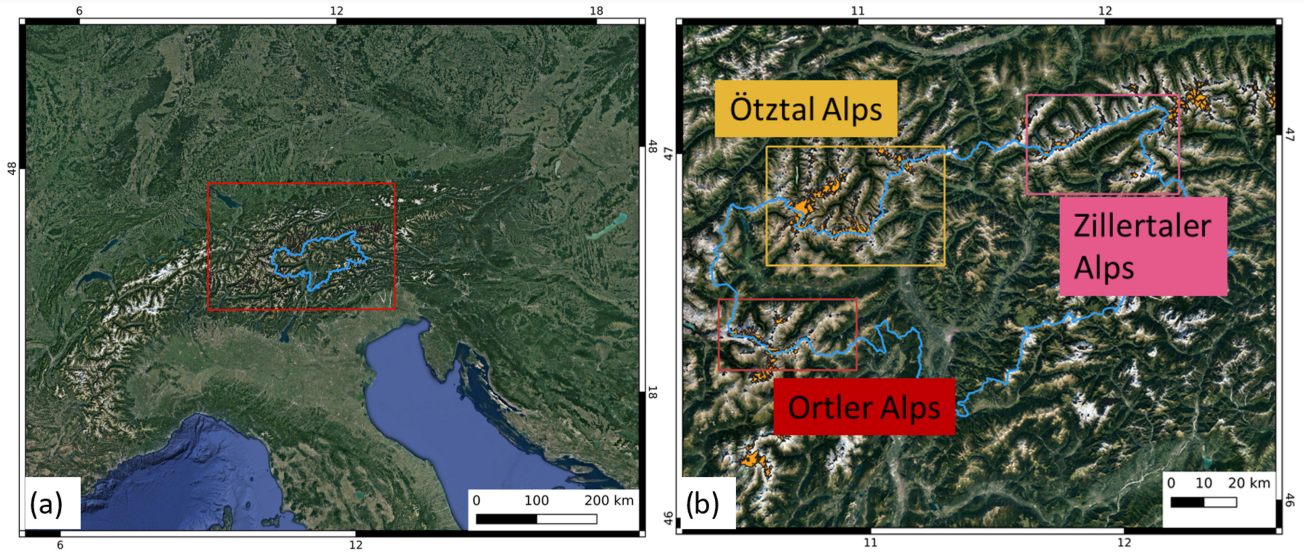


Fig. 1. Overview of the study area. In (a), the red box defines the area of application of the method, correspondent to six Sentinel-2 tiles, while the blue shape corresponds to the administrative limit of South Tyrol. In (b), a zoom over South Tyrol is reported. Ötztal Alps are highlighted in yellow, the Ortler Alps in red, and the Zillertaler Alps in pink.

TABLE I  
SATELLITE DATASET USED

Mission	Sensor Type	Tiles / Track	Processed Time Range
Sentinel-2	Optical Multispectral	32TPS, 32TPT,	July–September 2015
		32TNS, 32TNT,	July–September 2016
		32TQS, 32TQT	July–September 2017
Sentinel-1	SAR	15, 44, 95, 117, 198	July–September 2015 July–September 2016 July–September 2017

Group are included in tile 32TQT. Depending on the track overlap, the number of acquisitions covering these areas from July to September is 17 or 34. Regarding Sentinel-1 images, we selected five tracks for the study area (i.e., 15, 44, 95, 117, and 168 named using the ESA convention). They are partially overlapped, and in detail for South Tyrol, the Ortler Alps are covered by tracks 15, 117, and 168, the Ötztal Alps are covered by tracks 117 and 168 and partially by track 15, and the Zillertaler Alps are fully covered by tracks 44, 95, 117, and 168. For each track, one image every 12 days was acquired until 2016 and every six days since 2016. The data used are summarized in Table I. The European Union Digital Elevation Model over Europe (EU-DEM), [22], [23] was used for processing the Sentinel-1 data. This DEM is derived by the SRTM and filled with ASTER data to ensure a homogeneous processing over the alpine region.

### C. Reference Glacier Inventories

For the evaluation of our approach over the study area, we used 1) a high-resolution manually derived glacier inventory and 2) the glacier inventory of Alps derived from Sentinel-2 [16].

The dataset used for validation is summarized in Table II. The first inventory is available for the Ortler Alps and the Ötztal Alps (updated in 2016), and for the Zillertaler Alps (updated in 2017). These inventories were produced using the following multitemporal very high resolution data: 1) aerial orthophotos collected in 2016 and 2017 and 2) differential digital terrain models for 2005–2017. The DEMs were calculated from the ALS data collected in 2005 over the South Tyrol and the aerial photogrammetric survey of 2016 and 2017. The latter facilitated the delineation of glaciated areas, especially in areas covered by snow or debris [29], [30]. For the Ortler Alps, the University of Innsbruck made an ALS digital terrain model in 2013. The delineation of the glacier areas was done semi-automatically [31], [32]. Following the approach described in [29], the automatic processing was refined with manual post-processing using high-resolution shaded reliefs and orthoimages of 2016/2017 (scale 1:800) to increase the mapping accuracy. Debris-covered glacier areas were only considered in the 2017 inventory if the corresponding areas were classified as glaciers in a previously available inventory from 2005 and can still be identified as glaciated without a doubt based on the data for 2016/2017. Recently, Paul *et al.* [16] have published a glacier inventory derived from Sentinel-2 images. The method used by Paul *et al.* is significantly different from ours and primarily based on expert interpretation. The glaciers outlines were obtained by thresholding the red/short-wave infrared band (SWIR) band ratio [33] with different values for each date. The threshold is manually set to account for regional atmospheric conditions. An additional threshold on the blue band was used to remove misclassified rocks in shadows. Moreover, the satellite-based results were further manually refined to correct misclassification errors, including debris-covered glaciers and filling cloud gaps. No information from Sentinel-1 or other SAR instrument has

TABLE II  
REFERENCE DATASETS

	Ortler Alps	Ötztal Alps	Zillertaler Alps	Central East Alps
Year	2016	2016	2017	2015
Datasource	Aerial Images High-resolution DEMs Visual Interpretation	Aerial Images High-resolution DEMs Visual Interpretation	Aerial Images High-resolution DEMs Visual Interpretation	Sentinel-2 Visual Interpretation

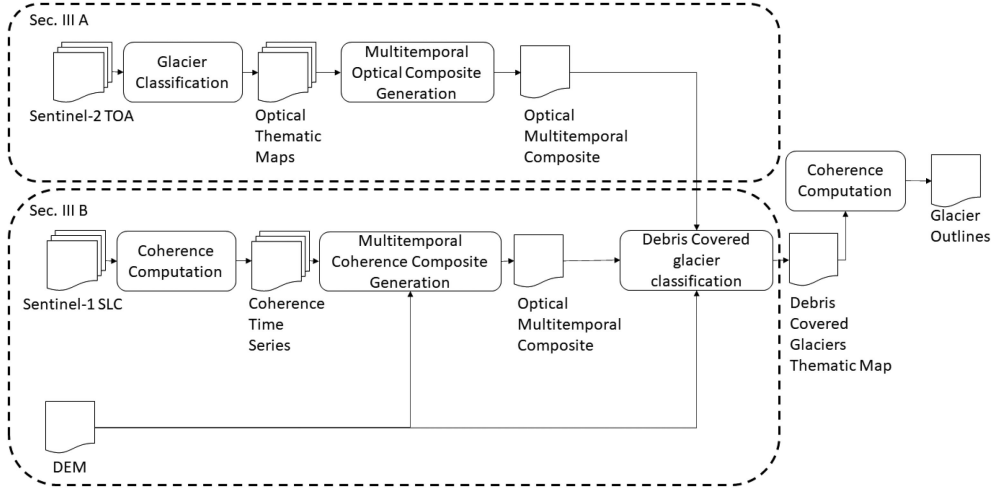


Fig. 2. Overview of the general workflow of the proposed method.

been employed. According to the authors, their outlines have uncertainties generally less than 5%.

### III. PROPOSED METHOD FOR GLACIER MAPPING

Let us consider two time series of 1) top-of-the-atmosphere Sentinel-2 images and 2) single-look complex Sentinel-1 images. The two time series cover the same geographic area and are acquired during the same ablation season. The Sentinel-2 time series is first classified into thematic maps representing the classes of bare ice ( $\omega_i$ ), snow ( $\omega_s$ ), water ( $\omega_w$ ), rock and debris ( $\omega_r$ ), and clouds ( $\omega_c$ ). These thematic maps are then composed in a single composite map with the lowest cloud and snow cover. In this way, the class snow can be semantically converted to glacier accumulation area. Next, the class of debris-covered glaciers ( $\omega_d$ ) is obtained from the Sentinel-1 time series. In detail, SAR coherence maps are computed for each image pair of the time series, with a certain temporal baseline. Then, the maximum of the coherence is selected pixelwise to compose the multitemporal coherence mosaic. The Sentinel-1 composite is obtained from different tracks to minimize the layover and shadow areas. The information extracted from the two composites is merged into a new thematic map with the following classes: glacier accumulation area ( $\omega_s$ ), bare ice ( $\omega_i$ ), debris-covered glacier ( $\omega_d$ ), and no-glacier ( $\omega_r$ ). Finally, the glacier outlines are generated by merging  $\omega_s$ ,  $\omega_d$ , and  $\omega_i$ . To speed up the processing, we limited the analysis to a spatial buffer of 0.5 km around the outlines of the Randolph Glacier Inventory version 6.0 [34], under the assumption that no new

glaciers were formed outside this buffer. This hypothesis is reasonable for the alpine glaciers after 2003 [16] and does not introduce any source of errors. Fig. 2 shows the workflow of the proposed method. In the following, the main steps are discussed into detail.

#### A. Optical Multitemporal Mosaic Generation

Several cloud detection approaches already exist for Sentinel-2 images, such as s2cloudless [35], [36], FMask [37], [38], or Sen2cor [39]. In this article, we used the s2cloudless algorithm. It is a supervised machine learning approach based on the gradient boosting of tree-based learning algorithms [40], which has been trained with 14 million samples from 596 Sentinel-2 tiles spread worldwide. We selected this algorithm because it demonstrated superior performances in a reference test set for cloud detection presented by Hollstein *et al.* [41]. More specifically, s2cloudless demonstrated to reduce the misclassification between cloud and snow by about 17% compared to Sen2cor and by about 26% compared to FMask [37], making this method more suitable for the monitoring of glaciers. S2cloudless requires three parameters: 1) a probability threshold to be applied to the cloud probability map (we used the default value of 0.4); 2) the size of the window for averaging the probabilities (we set this parameter to 2 pixels); and 3) the size of the morphological dilation filter (we set this parameter to 3 pixels). For the classification of snow, bare ice, water, rock, and debris, we propose a support vector machine (SVM) [42], [43] that exploits as features all the Sentinel-2 10-m spectral bands and the SWIR

B11 resampled from 20 to 10 m with bilinear interpolation, as suggested in [12]. The SVM was trained with an active learning process, starting from ten training samples collected for each of the semantic classes ( $\omega_i, \omega_s, \omega_r, \omega_c$ ); the training set is iteratively increased with additional manually collected training samples over the main misclassification errors spanning the entire time series [44]. Once generated the thematic maps for each acquisition time, the multitemporal composite is produced. This task first calculates the cleanliness index (CI) for each image pixel  $(i, j)$  not belonging to class clouds of each acquisition. In detail, the CI is computed using a square moving window with size  $W \times W$  as follows:

$$\text{CI}_{i,j}(t) = 1 - \frac{1}{W^2} \sum_{m=i-\frac{W}{2}}^{i+\frac{W}{2}} \sum_{n=j-\frac{W}{2}}^{j+\frac{W}{2}} c_{m,n}(t) \quad (1)$$

where  $t$  is the acquisition time,  $i$  and  $j$  are the pixel coordinates, and  $W$  is the size of the square window. In our study, we set a window size of 2 km ( $W = 200$  pixels) and  $c_{m,n}(t)$  is a binary mask defined as

$$c_{m,n}(t) = \begin{cases} 1, & \text{if } \begin{array}{l} (\text{thematic map}_{m,n}(t) \neq \omega_c) \\ \& \& \\ (\text{thematic map}_{m,n}(t) \neq \omega_s) \end{array} \\ 0, & \text{otherwise} \end{cases}. \quad (2)$$

Then, the composite map is made applying the following hierarchical criteria.

- 1) The higher the CI, the higher the probability for that pixel to be chosen for the final composite.
- 2) In the case of pixels with the same CI, to the image pixel with fewer neighboring pixels labeled as clouds in the  $W \times W$  window, a higher probability to be chosen for the final composite is assigned.
- 3) In the case of image pixels with both the same CI and amount of neighboring cloudy pixels, a higher probability to be used for the final composite is assigned to the image pixel from the most recent acquisition. If all the image pixels of the time series are cloudy in a specific location  $(i, j)$ , that location is set as no data in the composite map.
- 4) Finally, the optical multitemporal composite map is generated by assigning to each image pixel  $(i, j)$  the label of the pixel  $(i, j)$  of the time series with the highest probability.

## B. Coherence Multitemporal Composite Generation

Multispectral images are not suitable to identify parts of the glacier that are covered by debris [16]. On the other hand, the interferometric coherence provided by SAR systems can be used for this purpose, as proposed in [19]. In detail, SAR coherence  $\gamma$  is the phase noise of an interferogram between two SAR images  $S_1$  and  $S_2$  [45]. It can be computed as the cross-correlation coefficient of the SAR image pair estimated over an  $M \times N$  window in the image of column  $m$  and row  $n$  as

$$\gamma = \frac{\sum_{m=1}^M \sum_{n=1}^N S_1(m, n) S_2^*(m, n)}{\sqrt{\sum_{m=1}^M \sum_{n=1}^N |S_1(m, n)|^2 \sum_{m=1}^M \sum_{n=1}^N |S_2(m, n)|^2}} \quad (3)$$

where  $S_2^*$  is the complex conjugate of  $S_2$ . Unlike the approach presented in [19], which relies on a single coherence map, we used a multitemporal approach to exploit the coherence information. The coherence maps used come from different orbits, both ascending and descending, and are acquired during the entire ablation period. In addition, the information extracted from the Sentinel-2 multitemporal composite improved the detection. In detail, the first step for detecting debris-covered glaciers is the computation of the SAR coherence. This was done for all the Sentinel-1 image pairs with a temporal baseline of 12 days in the ablation season, which is a compromise between sensitivity to displacements and minimizes the temporal decorrelation noise. Data processing was performed using ESA's SNAP and the EU-DEM digital elevation model [46], [47]. All the coherence maps were derived using a  $19 \times 4$  pixel window. In the end, the coherences are geocoded and aligned with the extension of Sentinel-2 tiles. Geometrical distortion, including the layover and shadow effects, was masked out. In particular, pixels with local incidence angle smaller than  $35^\circ$  and greater than  $80^\circ$  were removed. The time series of coherence was used to generate the multitemporal coherence composite, representing the optimal condition to identify the surface displacements related to debris-covered glaciers. For this purpose, the highest coherence of the whole time series is calculated pixelwise as follows:

$$M = \underset{t}{\operatorname{argmax}}(\gamma(t)). \quad (4)$$

Consequently, all the transient factors that can lead to coherence loss are automatically filtered out (e.g., snow cover or rock falls) while preserving the effect of constant ground displacement induced by the glacier flow. Moreover, by exploiting the multiple acquisition geometries, we also obtain a SAR coherence composite where the geometric distortions, including shadow and layover, are minimized. However, some patches remain in layover or shadow due to the complex morphology of the area. Then, we masked all the pixels of the coherence multitemporal composite that were not classified as  $\omega_r$  in the Sentinel-2 multitemporal composite. Since we consider the coherence computed over rock and debris only, we assume that coherence losses are mainly caused by ground displacement. Indeed, all the other possible causes, such as volumetric scattering or noise due to low backscattering, are negligible over this specific land cover. For detecting the debris-covered glaciers, we then thresholded the SAR composite and terrain slope, generating pixelwise the thematic map  $d$  as follows:

$$d = \begin{cases} \omega_d, & \text{if } (\text{slope} < 30^\circ \text{ and coherence} < 0.5) \\ \omega_r, & \text{otherwise} \end{cases}. \quad (5)$$

Terrain slope was estimated with the EU-DEM and thresholded to  $30^\circ$ , as done in [19]. The coherence threshold is obtained using an expectation maximization algorithm, e.g., Gaussian mixture models [48]. However, experimental results showed that for our test sites, a threshold of 0.5 was a good tradeoff and can be adopted to speed up the whole procedure. Since isolated pixels occur in the map, we removed them by applying the morphological postprocessing operators opening (window size  $2 \times 2$  pixel), closing (window size  $4 \times 4$  pixel), and again opening

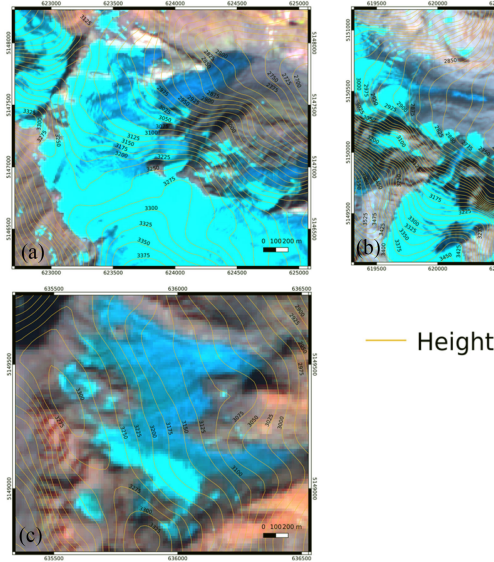


Fig. 3. Sentinel-2 multitemporal composites generated with the proposed method for (a) the Langferner, (b) the Suldenferner, and (c) the Weissbrunnenferner. Here, the composite is seen as RGB false color, with SWIR in red channel, NIR in green channel, and Green in blue channel.

(window size  $4 \times 4$  pixel), as suggested by Lippl *et al.* [19]. Finally, the debris-covered map from Sentinel-1 is merged with the glacier map from Sentinel-2. The final glacier outlines are obtained by semantically relabeling as glacier all the image pixels previously labeled as bare ice, glacier accumulation, and debris cover. All the other classes are relabeled as no-glacier.

#### IV. RESULTS AND DISCUSSION

According to the validation dataset, this section presents the outcomes for the Ortler Alps and Ötztal Alps for 2016, and the outcomes for the Zillertaler Alps for 2017.

##### A. Validation of the Proposed Glacier Mapping Method With Respect to a State-of-the-Art High-Resolution Dataset

In order to illustrate the outcomes of the proposed method, we focus on three different glaciers, Langferner as example of clean ice, Suldenferner as example of debris-covered glacier, and Weissbrunnenferner as cirque glacier, which have been studied since 1983. In detail, Fig. 3 shows the RGB false color of the composite over the three selected glaciers obtained, as described in Section III-A. More specifically, Langferner, Suldenferner, and Weissbrunnenferner are reported, respectively, in Fig. 3(a)–(c).

Fig. 4 shows the Sentinel-2 classified composite map for three glaciers. Fig. 5(a)–(c) shows the multitemporal coherence composite derived using (4) for Langferner, Suldenferner, and Weissbrunnenferner, respectively.

As one can notice, from these composites, it is possible to identify the whole glacier surface since they present low coherence, but it is not possible to clearly distinguish between the bare portion and the debris-covered portion of the glacier. According to the proposed method described in Section III-B, the coherence maps of Fig. 5 are classified using (5). Thus, debris-covered

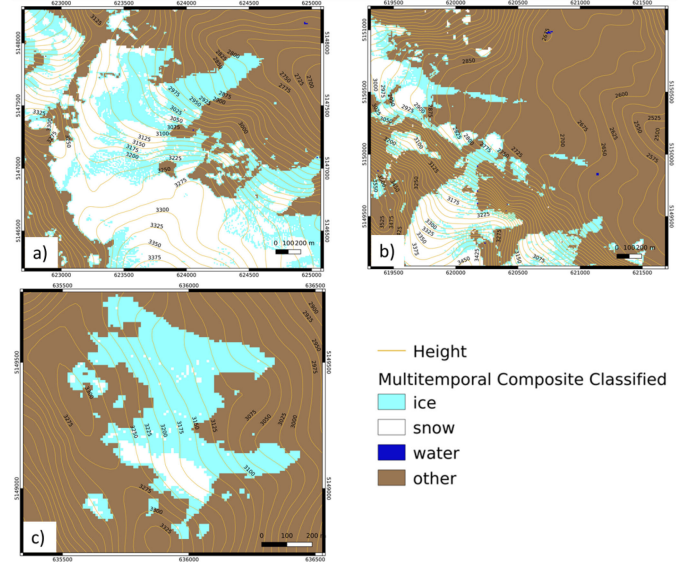


Fig. 4. Sentinel-2 multitemporal composites generated with the proposed method for (a) the Langferner, (b) the Suldenferner, and (c) the Weissbrunnenferner. Here, the composite is seen as thematic map.

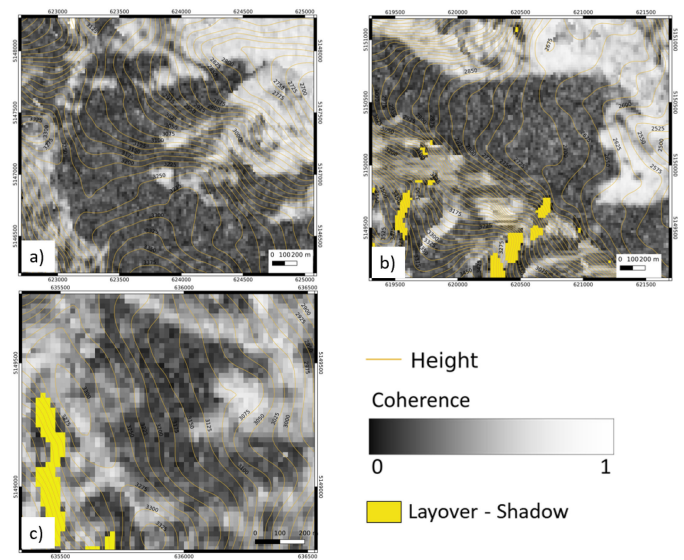


Fig. 5. Multitemporal coherence composites generated with the proposed method for (a) the Langferner, (b) the Suldenferner, and (c) the Weissbrunnenferner.

glaciers are detected by combining the Sentinel-2 and Sentinel-1 composite maps. Fig. 6 shows the final glacier maps superimposed to the reference glacier inventory. Qualitatively, one can notice a good agreement between the obtained maps and the reference outlines. The coarser resolution of Sentinel-1 composite is visible in the final map, especially for the Weissbrunnenferner [see Fig. 6(c)].

Table III summarizes the differences of the total glacier areas. Fig. 8 shows the confusion matrices, while Fig. 7 shows the glacier area difference for the three validation sites and for the whole South Tyrol. In order to ensure a balanced amount of testing samples for both glacier and no glacier, we added a buffer area around the reference glacier inventory.

TABLE III  
COMPARISON BETWEEN GLACIER EXTENT OF THE PROPOSED METHOD AND THE REFERENCE INVENTORY OVER SOUTH TYROL

Area Name	Glacier extent from S-2 [km <sup>2</sup> ]	Glacier extent from S-1 [km <sup>2</sup> ]	Glacier extent from S-2 + S-1 [km <sup>2</sup> ]	Reference glacier extent [km <sup>2</sup> ]	Difference [km <sup>2</sup> (%)]
Ortler Alps	28.5	7.8	36.3	34.0	+2.3 (+6.8%)
Ötztal Alps	26.5	9.2	35.7	31.8	+3.9 (+12.3%)
Zillertaler Alps	16.0	2.0	18.0	17.3	+0.7 (+4%)
South Tyrol	71.0	19.0	90.0	83.1	+6.9 (+8.3%)

TABLE IV  
COMPARISON BETWEEN GLACIER EXTENT OF THE PROPOSED METHOD AND THE GLACIER INVENTORY OF THE ALPS [17] OVER CENTRAL EAST ALPS

Area Name	Glacier extent from S-2 [km <sup>2</sup> ]	Glacier extent from S-1 [km <sup>2</sup> ]	Glacier extent from S-2 + S-1 [km <sup>2</sup> ]	Reference glacier extent [km <sup>2</sup> ]	Difference [km <sup>2</sup> (%)]
Central East Alps	483.8	146.6	630.4	608.2	+22.2 (+3.7%)

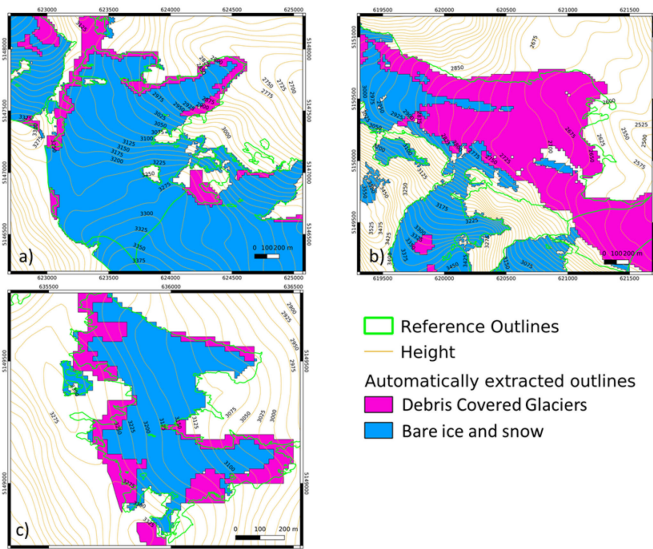


Fig. 6. Glacier maps obtained with the proposed method for (a) the Langferner, (b) the Suldenferner, and (c) the Weissbrunnenferner. Bare ice and snow are derived by Sentinel-2, while debris-covered glaciers are derived by Sentinel-1.

The Ortler Alps glaciers cover 34 km<sup>2</sup> according to the reference glacier inventories; using the optical multitemporal composite, we detected 28.5 km<sup>2</sup> since the debris-covered part cannot be recognized by the multispectral information. However, when merged with the information from Sentinel-1, the glacier surface covered by debris was correctly mapped, increasing the total area to 36.3 km<sup>2</sup>. The overall agreement changed from 65% to 92%, and the kappa coefficient raised from 0.75 to 0.83. Similarly to the Ortler case, also for the South Tyrolean part of the Ötztal Alps, by exploiting only the optical multitemporal composite, we underestimate the glacier area of 5.3 km<sup>2</sup>. The estimation improves when introducing the information of debris-covered glaciers derived from Sentinel-1 increasing the overall accuracy from 79% to 92% and the kappa coefficient from 0.81 to 0.86. The Zillertaler Alps area shows an overestimation of the glacier-covered area. The primary source of error is related to the persistent cloud coverage during the 2017 ablation season, which leads to the misinterpretation of

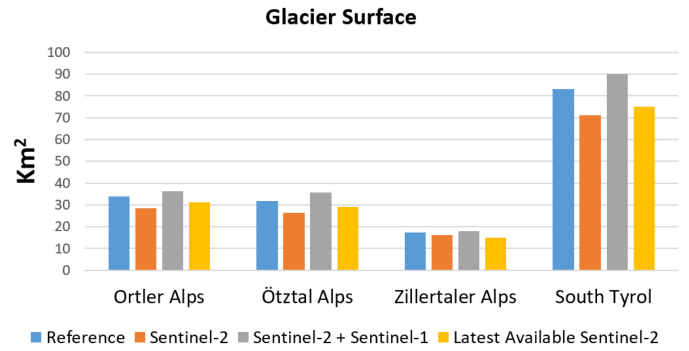


Fig. 7. Glacier surface in the three glacierized areas of South Tyrol according to the proposed automatic method and reference inventory.

some seasonal snow included in the glacier map. This represents the most common source of error for the method. Here, the improvement is 6% for the overall accuracy and 0.3 for the kappa coefficient. Finally, if we consider the whole South Tyrol, the glacier area mapped using the proposed method was 90.0 km<sup>2</sup>, while the reference inventory reported 83.1 km<sup>2</sup>. Thus, the overall accuracy is 91%, with an improvement of 16% compared to the mapping using only multispectral images (see Fig. 8). In that case, the kappa coefficient passes from 0.74 to 0.80.

#### B. Application of the Proposed Glacier Mapping Method to the Central East European Alps

The proposed method was then tested on the Central East Alps. As validation over this large area, we compared the obtained outlines with the latest glacier inventory available derived by Sentinel-2 [16]. In Table IV, the comparison in terms of area between the reference inventory and the output of our method is reported. According to the reference outlines, glaciers cover an area of 608.2 km<sup>2</sup>, while our method results show that glaciers cover an area of 630.4 km<sup>2</sup>. Fig. 9 presents the confusion matrix relative to the comparison of our method and the reference outlines. Part of the differences between the two inventories can be due to the sliding window used in coherence computation that reduces the spatial resolution, and due to the identification

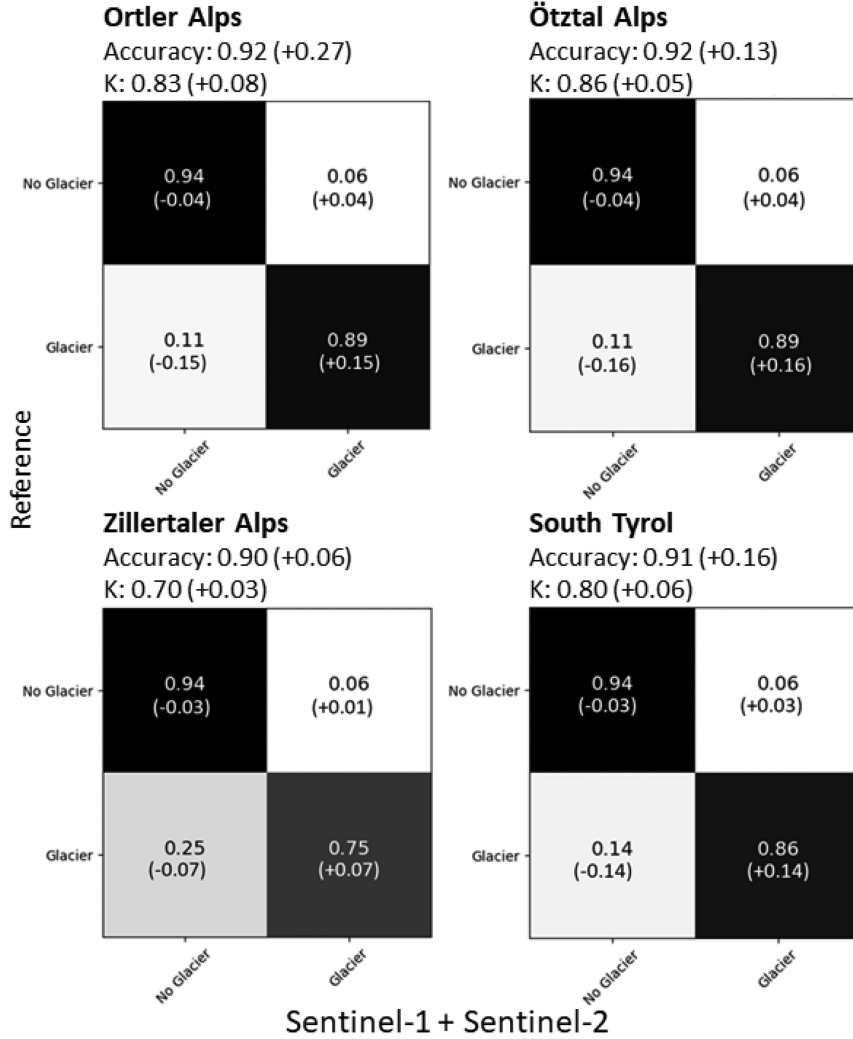


Fig. 8. Confusion matrices derived by the comparison between the reference glacier outlines and the results of the proposed method over South Tyrol. The relative changes after the merging of Sentinel-2 and Sentinel-1 composites compared to the accuracy obtained using the Sentinel-2 composite alone are in bracket.

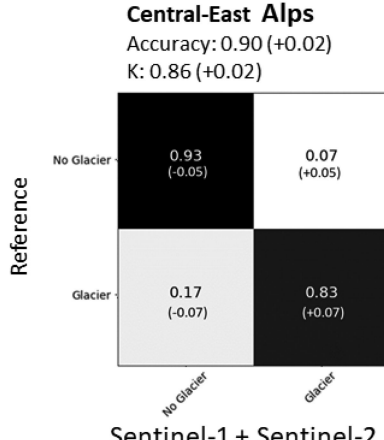


Fig. 9. Confusion matrices derived by the comparison between the glacier inventory of the Alps [16] and the results of the proposed method over Central Eastern Alps. The relative changes after the merging of Sentinel-2 and Sentinel-1 composites compared to the accuracy obtained using the Sentinel-2 composite alone are in bracket.

of rock glaciers, which are by definition not included in the glacier inventory used as reference. It is worth to note that the inventory used as reference is obtained with a high level of human supervision for the choice of the scene, the threshold definition, the snow patch filtering, and the debris-covered glacier identification. External datasets, e.g., orthophotos, have also been consulted for this refinement operation. On the other hand, the proposed method is fully automatic, and by exploiting free of charge, Sentinel images can provide a preliminary glacier mapping that can be used as a valuable starting point for updating glacier inventories.

## V. CONCLUSION

This article proposed a novel approach to exploit the large volume of data provided by Copernicus Sentinel missions for detecting glacier outlines, including debris-covered glaciers. In detail, our method exploits the Sentinel-1 and Sentinel-2 multitemporal images to build a composite image representing

the conditions during the yearly maximum ablation period. The Sentinel-2 multispectral images were classified with an SVM and composed to a mosaic that represents the information of the maximum glacier ablation. At the same time, the Sentinel-1 time series were exploited to build a multitemporal interferometric coherence composite, which represents all the snow-covered and glaciated areas, together with all the moving surfaces. This information was used together with the Sentinel-2 composite to detect the debris-covered part of the glaciers. We tested our methodology in the Central East Alps, in the area covered by six Sentinel-2 tiles. Over this large area, for 2015, we compared the method with the latest available glacier inventory derived by Sentinel-2 and manually edited for considering the possible presence of seasonal snow and debris-covered ice. Here the results show an overall agreement of 90%, with a difference on the area estimation of 3.7%. Furthermore, in South Tyrol (Italy), we evaluated the accuracy with the glacier inventories of 2016 and 2017 produced by glacier experts with field surveys, aerial orthophotos, and ALS data. Results show an overall accuracy of 92% with an error on the area of 8%. In that case, the assimilation of the debris-covered glacier information from Sentinel-1 contributed to an increase in the overall accuracy of 16% for the entire South Tyrol. This method presents a first step toward the complete automation of glacier mapping. The main limitation for the applicability of the method is related to the persistent cloud coverage over some areas. The cloud occlusion, in fact, can compromise the reconstruction with optical data of the glacier minimum snow cover situation. As future outlook, from the methodological point of view, we want to better investigate the glacier classification introducing the polarimetric SAR information. This will help to be more robust in the case of application in regions with persistent cloud cover. Other errors in the reconstruction can be introduced by the pixel misclassification. A consequent research outlook will be the correction of the time series exploiting the multitemporal information. From the application point of view, we want to use the developed method to perform some large-scale analysis. For instance, these automatically obtained inventories can be used as a starting point for an analysis of glacier changes over large areas and on a small time horizon, such as the whole Alps on a biennial basis. Moreover, we want to test the method over other glaciated areas, such as the Andes and the Himalaya.

## REFERENCES

- [1] L. Laurent *et al.*, “The impact of climate change and glacier mass loss on the hydrology in the Mont-Blanc massif,” *Sci. Rep.*, vol. 10, 2020, Art. no. 10420. [Online]. Available: <https://doi.org/10.1038/s41598-020-67379-7>
- [2] M. Beniston *et al.*, “The European mountain cryosphere: A review of its current state, trends, and future challenges,” *Cryosphere*, vol. 12, no. 2, pp. 759–794, 2018.
- [3] M. Hoelzle, W. Haeberli, M. Dischl, and W. Peschke, “Secular glacier mass balances derived from cumulative glacier length changes,” *Glob. Planet. Change*, vol. 36, no. 4, pp. 295–306, 2003.
- [4] L. M. Andreassen, H. Elvehøy, B. Kjøllmoen, R. V. Engeset, and N. Haakensen, “Glacier mass-balance and length variation in Norway,” *Ann. Glaciol.*, vol. 42, pp. 317–325, 2005.
- [5] D. Hall, J. Ormsby, R. Bindschadler, and H. Siddalingaiah, “Characterization of snow and ice reflectance zones on glaciers using landsat thematic mapper data,” *Ann. Glaciol.*, vol. 9, pp. 104–108, 1987.
- [6] R. Hock, D. S. Kootstra, and C. Reijmer, *Deriving Glacier Mass Balance From Accumulation Area Ratio on Storglaciären, Sweden*, P. Ginot and J. E. Sicart, Eds. Wallingford, U.K.: IAHS Press, 2007, pp. 163–170.
- [7] A. Linsbauer, F. Paul, and W. Haeberli, “Modeling glacier thickness distribution and bed topography over entire mountain ranges with GlabTop: Application of a fast and robust approach,” *J. Geophys. Res.: Earth Surf.*, vol. 117, no. 3, 2012, Art. no. F03007.
- [8] D. Farinotti, M. Huss, A. Bauder, M. Funk, and M. Truffer, “A method to estimate the ice volume and ice-thickness distribution of Alpine glaciers,” *J. Glaciol.*, vol. 55, no. 191, pp. 422–430, 2009.
- [9] B. S. Naz, C. D. Frans, G. K. C. Clarke, P. Burns, and D. P. Lettenmaier, “Modeling the effect of glacier recession on streamflow response using a coupled glacio-hydrological model,” *Hydrol. Earth Syst. Sci.*, vol. 18, no. 2, pp. 787–802, 2014.
- [10] A. Kääb *et al.*, “Glacier monitoring from ASTER imagery: Accuracy and applications,” in *Proc. EARSeL-LISSIG-Workshop Observ. Cryosphere Space*, 2002, vol. 2, pp. 43–53.
- [11] F. Paul, “Evaluation of different methods for glacier mapping using landsat TM,” in *Proc. EARSeL-SIG-Workshop Land Ice Snow*, 2000, pp. 239–245.
- [12] F. Paul *et al.*, “Recommendations for the compilation of glacier inventory data from digital sources,” *Ann. Glaciol.*, vol. 50, no. 53, pp. 119–126, 2009.
- [13] A. E. Racoviteanu, F. Paul, B. Raup, S. J. S. Khalsa, and R. Armstrong, “Challenges and recommendations in mapping of glacier parameters from space: Results of the 2008 Global Land Ice Measurements from Space (GLIMS) Workshop, Boulder, Colorado, USA,” *Ann. Glaciol.*, vol. 50, no. 53, pp. 53–69, 2009.
- [14] K. J. Bayr, D. K. Hall, and W. M. Kovalick, “Observations on glaciers in the Eastern Austrian Alps using satellite data,” *Int. J. Remote Sens.*, vol. 15, no. 9, pp. 1733–1742, 1994.
- [15] F. Paul, S. H. Winsvold, A. Kääb, T. Nagler, and G. Schwaizer, “Glacier remote sensing using Sentinel-2—Part II: Mapping glacier extents and surface facies, and comparison to landsat 8,” *Remote Sens.*, vol. 8, no. 7, 2016, Art. no. 575.
- [16] F. Paul *et al.*, “Glacier shrinkage in the Alps continues unabated as revealed by a new glacier inventory from Sentinel-2,” *Earth Syst. Sci. Data*, vol. 12, no. 3, pp. 1805–1821, 2020.
- [17] M. Callegari *et al.*, “A Pol-SAR analysis for alpine glacier classification and snowline altitude retrieval,” *IEEE J. Sel. Topics Appl. Earth Observ. Remote Sens.*, vol. 9, no. 7, pp. 3106–3121, Jul. 2016.
- [18] L. Huang, Z. Li, B.-s. Tian, J.-m. Zhou, and Q. Chen, “Recognition of supraglacial debris in the Tianshan mountains on polarimetric SAR images,” *Remote Sens. Environ.*, vol. 145, pp. 47–54, 2014.
- [19] S. Lippl, S. Vijay, and M. Braun, “Automatic delineation of debris-covered glaciers using InSAR coherence derived from X-, C- and L-band radar data: A case study of Yazgyl Glacier,” *J. Glaciol.*, vol. 64, no. 247, pp. 811–821, 2018.
- [20] B. A. Robson, C. Nuth, S. O. Dahl, D. Höglung, T. Strozzi, and P. R. Nielsen, “Automated classification of debris-covered glaciers combining optical, SAR and topographic data in an object-based environment,” *Remote Sens. Environ.*, vol. 170, pp. 372–387, 2015.
- [21] S. H. Winsvold, A. Kääb, and C. Nuth, “Regional glacier mapping using optical satellite data time series,” *IEEE J. Sel. Topics Appl. Earth Observ. Remote Sens.*, vol. 9, no. 8, pp. 3698–3711, Aug. 2016.
- [22] T. Loveland, J. Merchant, J. Brown, and D. Ohlen, “Development of a land-cover characteristics database for the conterminous U.S.,” *Photogrammetric Eng. Remote Sens.*, vol. 57, no. 11, pp. 1453–1463, 1991.
- [23] J. Cihlar, D. Manak, and M. D’Iorio, “Evaluation of compositing algorithms for AVHRR data over land,” *IEEE Trans. Geosci. Remote Sens.*, vol. 32, no. 2, pp. 427–437, Mar. 1994.
- [24] Q. Wang and J. D. Tenhunen, “Vegetation mapping with multitemporal NDVI in North Eastern China Transect (NECT),” *Int. J. Appl. Earth Observ. Geoinf.*, vol. 6, no. 1, pp. 17–31, 2004.
- [25] D. Roberts, N. Mueller, and A. McIntyre, “High-dimensional pixel composites from earth observation time series,” *IEEE Trans. Geosci. Remote Sens.*, vol. 55, no. 11, pp. 6254–6264, Nov. 2017.
- [26] S. Olen and B. Bookhagen, “Mapping damage-affected areas after natural hazard events using Sentinel-1 coherence time series,” *Remote Sens.*, vol. 10, no. 8, 2018, Art. no. 1272.
- [27] P. G. Minotti, M. Rajngewar, V. A. Santoro, and R. Grimson, “Evaluation of SAR C-band interferometric coherence time-series for coastal wetland hydropattern mapping,” *J. South Amer. Earth Sci.*, vol. 106, 2021, Art. no. 102976.

- [28] A. W. Jacob *et al.*, "Sentinel-1 InSAR coherence for land cover mapping: A comparison of multiple feature-based classifiers," *IEEE J. Sel. Topics Appl. Earth Observ. Remote Sens.*, vol. 13, pp. 535–552, 2020.
- [29] J. Abermann, A. Fischer, A. Lambrecht, and T. Geist, "On the potential of very high-resolution repeat DEMs in glacial and periglacial environments," *Cryosphere*, vol. 4, no. 1, pp. 53–65, 2010.
- [30] S. P. Galos *et al.*, "Recent glacier changes and related contribution potential to river discharge in the Vinschgau/Val Venosta, Italian Alps," *Geografia Fisica e Dinamica Quaternaria*, vol. 38, pp. 143–154, 2015.
- [31] M. Kodde, N. Pfeifer, B. Gorte, T. Geist, and B. Höfle, "Automatic glacier surface analysis from airborne laser scanning," in *Proc. ISPRS Workshop Laser Scanning*, 2007, pp. 221–226.
- [32] C. Knoll and H. Kerschner, "A glacier inventory for South Tyrol, Italy, based on airborne laser-scanner data," *Ann. Glaciol.*, vol. 50, no. 53, pp. 46–52, 2009.
- [33] F. Paul, A. Kääb, M. Maisch, T. Kellenberger, and W. Haeberli, "The new remote-sensing-derived Swiss glacier inventory: I methods," *Ann. Glaciol.*, vol. 34, pp. 355–361, 2002.
- [34] W. T. Pfeffer *et al.*, "The Randolph glacier inventory: A globally complete inventory of glaciers," *J. Glaciol.*, vol. 60, no. 221, pp. 537–552, 2014.
- [35] *Improving Cloud Detection With Mach. Learn.*, Sentinel Hub Blog, Medium. Accessed: Jun. 8, 2022. [Online]. Available: <https://medium.com/sentinel-hub/improving-cloud-detection-with-machine-learning-c09dc5d7cf13>
- [36] *Sentinel Hub Cloud Detect. for Sentinel-2 Images in Python*, Github, San Francisco, CA, USA. Accessed: Jun. 8, 2022. [Online]. Available: <https://github.com/sentinel-hub/sentinel2-cloud-detector>
- [37] Z. Zhu, S. Wang, and C. E. Woodcock, "Improvement and expansion of the Fmask algorithm: Cloud, cloud shadow, and snow detection for Landsat 4–7, 8, and Sentinel 2 images," *Remote Sens. Environ.*, vol. 159, pp. 269–277, 2015.
- [38] S. Foga *et al.*, "Cloud detection algorithm comparison and validation for operational landsat data products," *Remote Sens. Environ.*, vol. 194, pp. 379–390, 2017.
- [39] M. Main-Knorn, B. Pflug, J. Louis, V. Debaecker, U. Müller-Wilm, and F. Gascon, "Sen2Cor for Sentinel-2," *Proc. SPIE*, vol. 10427, 2017, Art. no. 1042704.
- [40] G. Ke *et al.*, "LightGBM: A highly efficient gradient boosting decision tree," in *Proc. Int. Conf. Neural Inf. Process. Syst.*, 2017, vol. 30, pp. 3146–3154.
- [41] A. Hollstein, K. Segl, L. Guanter, M. Brell, and M. Enesco, "Ready-to-use methods for the detection of clouds, cirrus, snow, shadow, water and clear sky pixels in Sentinel-2 MSI images," *Remote Sens.*, vol. 8, no. 8, 2016, Art. no. 666.
- [42] C. Cortes and V. Vapnik, *Support-Vector Networks Machine Learning*, vol. 20. Boston, MA, USA: Kluwer, 1995, pp. 237–297.
- [43] F. Melgani and L. Bruzzone, "Classification of hyperspectral remote sensing images with support vector machines," *IEEE Trans. Geosci. Remote Sens.*, vol. 42, no. 8, pp. 1778–1790, Aug. 2004.
- [44] D. Tuia, C. Persello, and L. Bruzzone, "Domain adaptation for the classification of remote sensing data: An overview of recent advances," *IEEE Geosci. Remote Sens. Mag.*, vol. 4, no. 2, pp. 41–57, Jun. 2016.
- [45] C. López-Martínez and E. Pottier, "Coherence estimation in synthetic aperture radar data based on speckle noise modeling," *Appl. Opt.*, vol. 46, no. 4, pp. 544–558, 2007.
- [46] *Copernicus Land Monit. Serv.* Accessed: Jun. 8, 2022. [Online]. Available: <https://land.copernicus.eu/imagery-in-situ/eu-dem/eu-dem-v1.1/view>
- [47] E. Józsa, S. Á. Fábián, and M. Kovács, "An evaluation of EU-DEM in comparison with aster GDEM, SRTM and contour-based DEMs over the Eastern Mecsek mountains," *Hung. Geograph. Bull.*, vol. 63, no. 4, pp. 401–423, 2014.
- [48] D. Reynolds, *Gaussian Mixture Models*. Boston, MA, USA: Springer, 2009, pp. 659–663.



**Riccardo Barella** received the M.Sc. degree in environmental engineering and the Ph.D. degree in environmental and infrastructure engineering from the Politecnico di Milano, Milan, Italy, in 2018 and 2022, respectively.

He is currently a Researcher with the Institute for Earth Observation, Eurac Research, Bolzano, Italy. His main research interests include cryosphere monitoring with earth observation data and its connection with hydrological processes.



**Mattia Callegari** received the M.Sc. degree in telecommunication engineering from the University of Trento, Trento, Italy, in 2012, and the Ph.D. degree in earth and environmental sciences from the University of Pavia, Pavia, Italy, in 2015.

He is currently a Researcher with the Institute for Earth Observation, Eurac Research, Bolzano, Italy. His main research interests include synthetic aperture radar and optical remote sensing of the alpine cryosphere and machine learning.



**Carlo Marin** received the M.Sc. degree in telecommunication engineering and the Ph.D. degree in information and communication technologies from the University of Trento, Trento, Italy, in 2011 and 2015, respectively.

He is currently a Senior Researcher with the Institute for Earth Observation, Eurac Research, Bolzano, Italy, where he is working in the framework of several national and international projects. His research interests include monitoring and understanding of the alpine cryosphere exploiting multitemporal and multisource remote sensing data.

Dr. Marin is a Referee for IEEE TRANSACTIONS ON GEOSCIENCE AND REMOTE SENSING, IEEE GEOSCIENCE AND REMOTE SENSING LETTERS, IEEE JOURNAL OF SELECTED TOPICS IN APPLIED EARTH OBSERVATIONS AND REMOTE SENSING, and *The Cryosphere*.



**Christoph Klug** received the B.Sc. degree in geo- and atmospheric sciences and the M.Sc. and Ph.D. degrees in geography from the University of Innsbruck, Tyrol, Austria, in 2008, 2011, and 2018, respectively.

He has contributed to a series of research projects in the field of remote sensing and cryospheric science at the Faculty of Geo- and Atmospheric Sciences of the University of Innsbruck (Institute of Geography and Inst. of Atmospheric and Cryospheric Sciences). His research mainly comprises different methods of remote sensing (e.g. LiDAR, photogrammetry, satellite remote sensing, etc.) and their application in cryospheric research, especially in glaciology.

**Rudolf Sailer** received the Ph.D. degree in geography (with a focus on physical geography) from the University of Innsbruck, Innsbruck, Austria, in 2002.

After the Ph.D., he was able to intensify his expertise in the field of avalanche research with the Institute for Avalanche and Torrent Research, Innsbruck. He was first a Project Leader and then a Senior Researcher with the Institute of Geography, University of Innsbruck, where he is currently a Senior Lecturer. His main research interests include physical geography (alpine cryosphere), natural hazard research, and short-range remote sensing, in particular the use of airborne and terrestrial laser scanning.



**Stephan P. Galos** received the Diploma in meteorology and geophysics and the Ph.D. degree in atmospheric sciences from the University of Innsbruck, Innsbruck, Austria, in 2010 and 2018, respectively.

He is currently with the University of Innsbruck. He has contributed to a series of research projects in the field of glaciology, micrometeorology, and glaciohydrology. His research interests include mass and energy exchange of glaciers and the seasonal snowpack, as well as related physical processes on various spatial and temporal scales.

**Roberto Dinale** received the bachelor's degree in environmental engineering from the University of Trento, Trento, Italy, in 1998, and the master's degree in land defense and maintenance from the University of Padua, Padua, Italy, in 2003.

He is currently the Director of the Hydrology and Dams Office, Autonomous Province of Bolzano—South Tyrol, Bolzano, Italy, and, therefore, responsible for quantitative hydrology and safety of dams in South Tyrol. He was the contact person for his institution for numerous European Regional Development Funds and Interreg projects. The study of the cryosphere and climate change completes the spectrum of his expertise. His main research interests include water cycle analysis and monitoring to hydrological modeling and forecasting, both short-term and seasonal, to the management of water resources and natural hazards.

Mr. Dinale is a Member of various bodies and associations, including the Italian National Table of Operational Hydrology, the District Observatory of the Eastern Alps on Water Uses, the Italian Glaciological Committee, IT-Cold, and the Scientific Advisory Board of the Eurac Institute for Earth Observation.



**Marco Gianinetto** received the M.S. degree in environmental and land management engineering and the Ph.D. degree in geodesy and geomatics from the Politecnico di Milano, Milano, Italy, in 2006 and 2010, respectively.

He is currently an Associate Professor of Geomatics with the Politecnico di Milano and an Associate with the Institute for Electromagnetic Sensing of the Environment, National Research Council of Italy, Rome, Italy. His research interests include remote sensing technologies, earth observation, spatial information sciences, and data science.

Prof. Gianinetto is a Member of the Governing Council of the Italian Remote Sensing Society, a Co-Editor-in-Chief for *European Journal of Remote Sensing*, and an Associate Editor for *Journal of Remote Sensing* and *Journal of Applied Remote Sensing*. He has been a member of several international advisory/evaluator panels, including the Executive Agency for Small and Medium-sized Enterprises and the European Health and Digital Executive Agency of European Commission, the Italian Ministry of Universities and Research, the Israel Science Foundation, the National Research Council of Romania, the Belgian Federal Science Policy Office, and the French National Research Agency, and a mentor for the EU Copernicus Accelerator coaching program.



**Claudia Notarnicola** (Senior Member, IEEE) received the M.S. degree in physics (*summa cum laude*) and the Ph.D. degree in physics from the University of Bari, Bari, Italy, in 1995 and 2002, respectively.

She is currently the Vice-Head of the Institute for Earth Observation, Eurac Research, Bolzano, Italy, where she is also the Leader of a group dealing with remote sensing applications in the synthetic aperture radar (SAR) and optical domain for soil, snow, and vegetation monitoring, as well as integration of remotely sensed observations with models and ground measurements. She conducts research within the frameworks of several national and international projects. Among others, she was also involved in the Cassini–Huygens Mission for the application of an inversion procedure to the estimation of Titan surface parameters. Her research interests include biophysical parameter (soil moisture, vegetation, and snow) retrieval using optical and SAR images, optical and SAR data processing, data fusion, and electromagnetic models.

Dr. Notarnicola has been a Conference Chair for SPIE International Conference on Active and Passive Microwave Remote Sensing for Environmental Monitoring since 2006.